



1 **Expanding Limits of Laser-Ablation U-Pb Calcite Geochronology**

2 Andrew R.C. Kylander-Clark

3 Department of Earth Science, University of California, Santa Barbara, CA 93106, USA.

4 *Correspondence to:* Andrew R. C. Kylander-Clark (akylander@ucsb.edu)

5 **Abstract.** U-Pb geochronology of calcite by laser-ablation inductively-coupled mass spectrometry (LA-
6 ICMPS) is an emerging field with potential to solve a vast array of geologic problems. Because of low
7 levels of U and Pb, measurement by more sensitive instruments, such as those with multiple collectors
8 (MC), is advantageous. However, whereas measurement of traditional geochronometers (e.g., zircon) by
9 MC-ICPMS has been limited by detection of the daughter isotope, U-Pb dating of calcite can be limited
10 by detection of the parent isotope, if measured on a Faraday detector. The *Nu P3D* MC-ICPMS employs a
11 new detector array to measure all isotopes of interest on Daly detectors. A new method, described herein,
12 utilizes the low detection limit and high dynamic range of the *Nu P3D* for calcite U-Pb geochronology,
13 and compares it with traditional methods. A model is created to explore the limits of U, Pb, and U/Pb
14 ratios that can be measured by LA-ICPMS and can serve as a guide to evaluate potential candidate
15 materials for geochronology.

16 **1. Introduction**

17 Calcite U-Pb geochronology by laser-ablation inductively-coupled mass spectrometry (LA-ICPMS) is a
18 relatively new technique with untapped potential for solving numerous geochronologic problems from the
19 timing of faulting (e.g., Roberts and Walker, 2016; Nuriel et al., 2017; Goodfellow et al., 2017), age of
20 ore deposits (Burisch et al., 2017) to paleoclimate, sedimentation, and diagenesis (e.g., Manganot et al.,
21 2018; Rasbury et al., 1997; Hoff et al., 1995; Winter and Johnson, 1995; Wang et al., 1998; Rasbury et
22 al., 1998). Early studies focused on carbonates more likely to contain high concentrations of U, such as
23 speleothems (e.g., Richards et al., 1998) because the method employed—thermal ionization mass
24 spectrometry (TIMS)—required weeks to produce reliable ratios; samples with a low likelihood of
25 success, that is, those with potentially low U contents, were ignored. With the advent of LA-ICPMS,
26 however, sample throughput and analytical costs have been greatly reduced, such that hundreds of



27 geanalytical facilities can, at the very least, screen a large number of samples and choose those suitable
28 for geochronology in a relatively short period of time and for little cost. Actual analysis time and cost are
29 also reduced over TIMS—sample preparation is minimal and several samples can be analyzed in a day—
30 and dozens of labs worldwide have the capability to perform such analyses. LA-ICPMS also has the
31 advantage of sampling smaller volumes of material; it can thus take advantage of the heterogenous nature
32 of calcite with respect to U and Pb, using larger datasets to better constrain both the initial $^{207}\text{Pb}/^{206}\text{Pb}$
33 compositions and the common Pb-corrected concordia ages. These isochron ages are calculated with ease
34 on a Tera-Wasserburg diagram similar to other common-Pb-bearing mineral chronometers like titanite
35 and apatite (e.g., Chew et al., 2014; Spencer et al., 2013).

36 For typical LA-ICPMS analyses, a 193 nm excimer laser is employed in conjunction with either a single-
37 collector (SC-ICPMS), or multi-collector (MC-ICPMS) sector-field instrument to take advantage of the
38 increased sensitivity over a quadrupole (Q-ICP-MS). Traditionally, an MC-ICPMS uses a series of
39 Faraday detectors on the high-mass side of the detector array to measure ^{238}U and ^{232}Th , and either
40 Faraday cups or secondary electron multipliers (SEMs) on the low-mass side of the array to concurrently
41 measure Pb isotopes; SC-ICPMS instruments measure isotope count rates sequentially with a single SEM.
42 The SC and MC instruments have distinct advantages. Because there is only one SEM on a SC-ICPMS
43 instruments, there is no need to cross calibrate multiple detectors, yielding simpler data reduction and the
44 possibility for making 204- or 208-based common-Pb corrections. An MC-ICPMS, on the other hand, is
45 2–3 times more sensitive than the top SC-ICPMS instruments. This allows precise measurements of
46 samples with low levels of Pb (i.e., young and/or low common-Pb). Furthermore, its *equivalent* sensitivity
47 is even higher because it measures all masses at the same time. For example, a SC-ICPMS running only
48 masses 238, 207, and 206 (232, 208, and 204 are also typically measured) at equal dwell times measures
49 1/3 the counts over a given cycle than the count rate might suggest because only one mass can be
50 measured at a time; given that it is also 2-3x less sensitive than an MC-ICPMS, a laser spot must be ~6-9
51 times bigger to achieve the same precision on a SC-ICPMS. A further advantage of an MC-ICPMS is that



52 transient signals from changes in U and Pb concentration during ablation affect uncertainties in the
53 measured $^{207}\text{Pb}/^{206}\text{Pb}$ and $^{206}\text{Pb}/^{238}\text{U}$ less because all measurements are made concurrently. Finally, the
54 smaller dynamic range of the SEM can limit samples to a specific range of U concentrations; samples or
55 reference materials with high U contents can cause the detector to trip to a different measurement mode
56 (or trip off), yielding spurious results. Low U concentrations in calcite can also be a problem for an MC-
57 ICPMS measuring ^{238}U with a Faraday cup because limits of detection are on the order of 10^4 cps. Even
58 though the SC-ICPMS has 2–3 times lower sensitivity than an MC-ICPMS, it can precisely measure
59 count rates of $\sim 10^2$ cps by employing a secondary electron multiplier (SEM) for all masses. Because of its
60 reduced sensitivity, however, this equates to a very small range of samples.

61 Fortunately, a recently introduced MC-ICPMS—the *P3D*—by *Nu Instruments* (Wrexham, UK) can
62 overcome both of these limitations. The instrument features a Daly detector array that allows for ion
63 counting on ^{238}U and the Pb isotopes, and thus expands the range of calcite samples—those with lower U
64 concentrations—that can be precisely measured by LA-ICPMS. Not only does a Daly detector increase
65 the sensitivity of the instrument, but unlike a standard SEM, the Daly has a greater dynamic range
66 (approx. 10-fold over that of an SEM) and can thus be used with a larger range of U concentrations. This
67 contribution describes the analytical setup for LA-ICPMS using the new *Nu P3D*, comparing the two
68 modes with each other and with that of a SC-ICPMS, and thereby demonstrating the increased capability
69 of this new instrumentation to measure calcite U-Pb dates.

70 **2 Experimental Setup**

71 The analytical setup is described in Table 1. The instrumentation used in the study consists of a *Photon*
72 *Machines Excite* 193 nm excimer laser equipped with a HelEx cell, coupled to a *Nu Instruments P3D* for
73 standard LA-ICPMS analyses. The *Nu Plasma 3D (P3D)* contains an array with 6 Daly detectors, 5 on the
74 low-mass side of the array and 1 on the high-mass side. A 14-Faraday array lies between the Daly
75 detectors, and allows for measurement of ^{238}U on either a Faraday or Daly detector, depending on the U
76 concentration in the sample. Daly detectors are used to measure masses 202, 204, 206, 207, and 208, and



77 ^{232}Th is measured on a Faraday cup. Faraday backgrounds yield a 1SD of 0.04 mV, which implies a limit
78 of detection (LOD) of ~0.1 mV or ~8000 cps; Daly backgrounds yield 1SD of 10–20 cps for isotopes of
79 Hg and Pb and 1 cps for ^{238}U , corresponding to LODs of 30–60 and 3 cps, respectively.

80 In order to compare the difference between SC and MC analytical sensitivities and uncertainties, the laser
81 was used in conjunction with the *P3D* for two experiments, and an *Agilent 7700 Q-ICPMS* for one
82 experiment. These 3 experiments were run with different spot sizes: *Experiment F*) a 65 μm spot on the
83 *P3D* using a Faraday for masses 238 and 232, and Daly detectors for masses 208–204 and 202 (110 total
84 analyses); *Experiment D*) the same configuration, but with 238 measured on a Daly detector; and
85 *Experiment Q*) a 110 μm spot with the Q-ICPMS and cycle times of 0.06, 0.13, 0.1, and 0.1 s on masses
86 238, 207, 206, and 204 respectively. During each separate analytical run, each spot was located near the
87 corresponding spot from the other runs, to minimize uncertainty caused by grain homogeneity. For all
88 experiments, the laser was run at 10 Hz for 15 seconds and a fluence of approximately 1 J/cm^2 , yielding a
89 spot depth of 10–15 μm . Analyses were preceded by two pre-ablation pulses, and 20 seconds of baseline
90 measurement.

91

92 Three calcite samples from the east coast of North America (courtesy of W. Amidon of Middlebury
93 College) were the main samples measured. These samples—C258, C304, and C273—are ca. 440, 110,
94 and 80 Ma, respectively, and range in U concentration between a few ppb and a few ppm, with an average
95 of 120 ppb and a mode of ~20 ppb. Three further samples (C254, C283A, and C283B), were run in
96 experiments F and D and provide more data for uncertainty comparisons between the two instrumental
97 configurations (see Figure 1), but the data are described in less detail; they are ca. 440 Ma with variable
98 Cretaceous (?) (re)crystallization. Calcite and NIST614 reference materials (RMs) were interspersed
99 every 10 analyses, and a two-stage reduction scheme was employed. *Iolite v.3.0* (Paton et al., 2011) was
100 used first used to correct the $^{207}\text{Pb}/^{206}\text{Pb}$ for mass bias, detector efficiency, instrumental drift etc., and to



101 correct the $^{238}\text{U}/^{206}\text{Pb}$ ratio for instrumental drift, using NIST614 as the primary reference material.
102 During this first data reduction, 2 seconds were removed from both the beginning and end of both the
103 RMs and the unknowns, yielding a total count time of 11 s. The $^{238}\text{U}/^{206}\text{Pb}$ ratio was then corrected using
104 a linear correction in *Excel* such that the primary calcite RM, WC-1, yielded 254 Ma (Roberts et al.,
105 2017) on a Tera-Wasserburg (TW) diagram, anchored to a $^{207}\text{Pb}/^{206}\text{Pb}$ value of 0.85. Using this method,
106 we retrieved ages of 3.01 ± 0.15 (MSWD = 1.3; n = 30) and 65.9 ± 1.1 (MSWD = 1.2; n = 40) for
107 secondary RMs ASH15 (2.96 Ma; Nuriel et al., in review) and Duff Brown Tank (64 Ma; Hill et al.,
108 2016), respectively. Analyses with large uncertainties (arbitrarily chosen as 50% for both $^{238}\text{U}/^{206}\text{Pb}$ and
109 $^{207}\text{Pb}/^{206}\text{Pb}$) were discarded; removing these data has little influence on the final age. The data from the
110 unknowns are all a bit scattered for geological reasons, and were culled to yield single populations for
111 ease of comparison. (Though beyond the scope of this manuscript, the Paleozoic samples are interpreted
112 to have suffered partial Pb loss or new crystal growth in the Cretaceous–Tertiary, and the older
113 Cretaceous sample likely (re)crystallized over an extended period.)

114 **3 Results**

115 Table 2 and Figure 2 shows the results for the 6 samples analyzed in the 3 experiments. *Experiment F*
116 (*P3D* – 65 μm spot; *U* on a *Faraday*) yielded ~2.7 mV/ppm of mass 238 on NIST614 and was relatively
117 stable throughout the run. The sensitivity of *Experiment D* (*P3D* – 65 μm spot; *U* on a *Daly*) was similar
118 to that of *Experiment F*, but dropped approximately 25% during the analytical session to ~2 mV/ppm of
119 mass 238 on NIST614. *Experiment Q* (*Agilent Q-ICPMS* – 110 μm spot) yielded ~110 kcps/ppm of mass
120 238 on NIST614—equivalent to ~1.8 mV/ppm from a spot ~3 times larger than the 65 μm spot in
121 experiments 1 and 2—and was stable throughout the run.

122 For every sample, Experiment F yielded fewer analyses with uncertainties of <50% for $^{206}\text{Pb}/^{238}\text{U}$, as well
123 as the fewest spots available to make an isochron. These results are consistent with a higher average and
124 median U ppb; low U concentrations that were measured in Experiments D and Q went undetected or
125 yielded large uncertainties in Experiment F. Though samples with median ^{238}U count rates of >10,000 cps



126 (C273C and C304A) returned fewer viable analyses and worse average $^{238}\text{U}/^{206}\text{Pb}$ uncertainties in
127 Experiment F, the uncertainty of the final age was similar for the higher-U samples on both
128 configurations on the *P3D*; both yielded lower uncertainties than the Q-ICPMS, despite the 3-fold volume
129 increase in analyzed material on the Q-ICPMS.

130 When average count rates of ^{238}U were below ~8000 cps (near the detection limit of the Faraday detector
131 on the *P3D*), however, the number of viable analyses and final age uncertainty was significantly higher in
132 Experiment D (Table 2 and Figure 2). As an example, sample C258 yielded few viable data points (35%
133 of the 110 analyses) in Experiment F, fewer than half the number of good analyses in Experiments D and
134 Q. In addition, the resulting uncertainty in the final age calculation (~4%) is significantly larger than that
135 of Experiment D, and similar to the resulting uncertainty in Experiment Q (although the Q-ICPMS
136 yielded >2 times the number of viable spots). Samples C283A and C283C—which also contain low levels
137 of U—yielded ~50% fewer viable data, necessitated double the average count rates of ^{238}U , and final
138 uncertainties that were significantly greater in Experiment F than those of Experiment D.

139 A summary of the precision vs. U count rate is shown in Figure 1, which shows the precision of $^{238}\text{U}/^{206}\text{Pb}$
140 and ^{238}U on a single spot vs. the count rate of ^{238}U . While there is considerable overlap in the precision vs.
141 ^{238}U cps of both ^{238}U and $^{238}\text{U}/^{206}\text{Pb}$ at count rates above approx. 30,000 cps, data collected in Experiment
142 F yielded no better than a few kcps 2σ uncertainty on ^{238}U ; $^{238}\text{U}/^{206}\text{Pb}$ uncertainties consequently show a
143 similar deviation from the high-count-rate trend. Finally, though the Q-ICPMS shows similar gains in
144 precision for low-U analyses, the lower sensitivity of the Q-ICPMS results in a minor window of U
145 concentrations for which analyses have lower uncertainties than those run on the *P3D*.

146 **4 Discussion**

147 While there is a clear advantage of using the new Daly-only detector setup on the *P3D* for LA-based
148 calcite geochronology for some samples, the extent to which this advantage obtains for all samples is still
149 somewhat ambiguous. The samples that benefit most from the new instrumentation are not only low in U,



150 but also older. For most measurements of long-lived-isotope geochronology, the analytical limit is
151 determined by the detection limit of the daughter, not the parent, isotope. However, because older
152 samples have more daughter product, they are—for samples with low U/Pb_c ratios—analyses of those
153 samples are more likely to be limited by the count rate of the parent isotope. For samples run on a SC-
154 ICPMS, this distinction is unimportant because the detection limit of ^{238}U is in all cases lower than that
155 for Pb. However, because the MC-ICPMS has a large sensitivity and precision advantage over the SC-
156 ICPMS, it is important to distinguish the limits of measurement between the Faraday–Daly and all-Daly
157 configuration.

158 **4.1 Theoretical uncertainty of Tera–Wasserburg data**

159 To explore the limits of precision for each analytical configuration, a dataset was created to represent
160 different U/Pb_c and ^{238}U cps for samples of different ages. Figure 3 shows samples with ages of 440, 80,
161 and 15 Ma with error ellipses at U/Pb_c ratios of 1, 2, 5, 10, 20, 100 and 200. The size of the ellipse is the
162 maximum possible uncertainty (from counting statistics only) for a 10s analysis, given the limit of
163 detection of the instrument. For the all-Daly configuration, the limit of detection is determined by ^{207}Pb
164 counts, the least abundant isotope of interest. For this example, 30 cps is assumed (the best achieved
165 LODs herein; Gerdes et al), but it is important to recognize that the LOD of Pb is based on the
166 background, which varies from lab to lab, and is also a function of the instrumental sensitivity. For the
167 Faraday–Daly arrangement, the LOD is limited by ^{238}U counts for samples with lower U/Pb_c and by ^{207}Pb
168 for samples with high U/Pb_c —and increasingly so as the sample age decreases. In this case, a minimum of
169 30,000 cps of ^{238}U is considered—as opposed to the actual ca. 8000 cps LOD—for the Faraday, because
170 that is the count rate below which a distinct benefit in precision is gained by using the all-Daly
171 arrangement (see Figure 1 and discussion above). As depicted in Figure 3, older samples yield the greatest
172 range of U/Pb_c ratios that could yield an advantage of measurement by ^{238}U on an ion counter, whereas
173 the advantage of the Daly detector disappears at U/Pb_c ratios greater than ca. 500 and 250 for samples that
174 are 80 and 15 Ma, respectively. As an example of the benefit of ^{238}U measurement by Daly, an 80 Ma



175 sample with a maximum U/Pb_c ratio of 10 yields 1400 cps of ²³⁸U at the LOD of 30 cps ²⁰⁷Pb. Given a
176 limit of detection of 8000 cps for the Faraday detector, the signal size would need to be 6 times higher
177 before it could be measured by such means. Furthermore, as discussed above, and shown in Figure 1, the
178 benefit of the Daly extends to ca. 30,000 cps, or ~20 times the signal that can be measured by the
179 Faraday–Daly configuration. The benefit extends to 200 times for a U/Pb_c ratio of 1; but some question
180 arise as to the ability to measure ages at such low U/Pb_c values.

181 **4.2 Choosing Samples and Instruments**

182 One intention of this manuscript is to serve as a guide to determine whether any given calcite (or any
183 other Pb_c-bearing) sample is appropriate for U–Pb geochronology, and deciding which type of analytical
184 equipment to use. As such, the model above is expanded below to explore the U/Pb_c ratios and count rates
185 needed to produce a reliable age from a given number of analyses. These models are then compared with
186 the natural results to determine best practices when selecting samples and instruments for analysis.

187 Calculating theoretical limits is complicated, however, because the uncertainty of an isochron depends on
188 the distribution of U, Pb_c, and thus the distribution of U/Pb and Pb/Pb ratios. For example, a sample with
189 a given maximum U/Pb_c will yield a final precision that increases with the number of analyses, but this
190 improvement depends on the distribution of the U/Pb_c ratios. The distribution of U and Pb, and thus
191 ²³⁸U/²⁰⁶Pb and ²⁰⁷Pb/²⁰⁶Pb, in calcite has not been a particular subject of study, but a cursory analysis of
192 the reference materials and unknowns presented in this manuscript shows that U and Pb concentrations
193 follow normal distributions; RMs that contain sufficient U (WC-1 and Duff Brown Tank) display a near-
194 normal distribution of U, whereas the distribution of U concentration of samples and RMs with lower U
195 contents (ASH15 and unknowns) are log normal (Figure 4). Like U, Hg-corrected ²⁰⁴Pb counts (a proxy
196 for common Pb) are normally distributed in RMs and unknowns; ²⁰⁸Pb counts are similar. The resulting
197 ²³⁸U/²⁰⁶Pb ratios of RMs are normally distributed, but unknowns vary and can be rather uniform (e.g.,
198 C273C). The manner by which the type of distribution affects the final uncertainty is demonstrated in
199 Figure 5. The precision of a T-W isochron is best defined by precisely defined end points with maximum



200 spread; as such, except for samples with extreme U/Pb_c , a uniform distribution of $^{238}U/^{206}Pb$ ratios results
201 in better final age precision than does a normal distribution. For example, a sample that is 440 Ma with
202 normally distributed data (and ratios $\pm 3\sigma$ from the mean) requires nearly 2 times as many points to
203 achieve the same precision as a sample with uniformly distributed data over the same U/Pb range (though
204 this also depends on the maximum U/Pb_c). For normally distributed data with the same maximum U/Pb_c ,
205 but only 50% of the spread (i.e., more tightly clustered; Figure 5b), the number of necessary data points
206 increases further, excepting samples with extreme U/Pb_c (these data would be less dependent on the
207 precision of the upper intercept).

208 To compare theoretical data with that obtained from this study—i.e., in order to best represent a natural
209 dataset—we present and discuss models with 100 uniformly distributed $^{238}U/^{206}Pb$ data points acquired for
210 10 s at 10 Hz, recognizing that, as stated above, this is likely a best-case scenario. We explore the
211 implications of varying maximum U/Pb_c ratios rather than $^{238}U/^{206}Pb$ ratios because the former are
212 independent of sample age. The results of the model are shown in Figure 6 Because the precision of
213 analyses in an ion-counter-only configuration is limited by the count rate of ^{207}Pb , we calculate the
214 maximum U/Pb_c ratio that can be achieved for different concentrations of U. For example, a 440 Ma
215 sample with 10 ppb U run with a 65 μm spot size will yield ~ 1500 cps of U. The maximum U/Pb_c that
216 could be achieved with this count rate will be ~ 13 , because any higher values will yield too few counts of
217 ^{207}Pb to be measured. Assuming constant U concentration and normally distributed $^{238}U/^{206}Pb$ ratios, the
218 best precision on the age of this sample is 0.6%—considerably better than expected for LA-ICPMS (e.g.,
219 Horstwood et al., 2016). As a comparison, sample C283A contains an average of 10 ppb U (and
220 maximum of 40 ppb) and thus yields a similar average count rate of ^{238}U . Its maximum U/Pb_c of 26 is
221 considerably less than the maximum theoretical value based on the concentration of that particular
222 analysis because its Pb concentration is well above detection. It should be no surprise then, that the age
223 uncertainty is higher than the theoretical value at that count rate, but it is also higher than the theoretical
224 value for a U/Pb_c of 26. Several factors may explain this: 1) though 100 analyses were measured, 32 were



225 imprecise and rejected; 2) the distribution of $^{238}\text{U}/^{206}\text{Pb}$ ratios is not uniform; 3) laser instability, detector
226 response time, laser-induced elemental fractionation (LIEF), signal instability, etc. add uncertainty
227 beyond that based on counting statistics; and 4) low U/Pb_c values likely have less U and Pb than in the
228 model.

229 Although optimistic, this model serves as a guide for the limitation of analyses of calcite by LA-ICPMS,
230 given U concentration, maximum U/Pb_c , and spot size. First, for all but the youngest samples ($\ll 15$ Ma),
231 measurement with the *P3D* can be advantageous for samples with lower U or those necessitating small
232 spot sizes (e.g., <150 ppb U and <65 μm ; <50 ppb U and <125 μm). However, if, for example, the sample
233 contains concentrations >100 ppb U and the spot can be >100 μm , there is no advantage to using the all-
234 Daly configuration, and if there is significant material (i.e., spot size can be >200 μm), any LA-ICPMS
235 will provide the best possible results (that is, the precision will be limited not by the count rate, but rather
236 other factors such as differences in LIEF, matrix effects etc.). Second, it is highly unlikely that even with
237 extreme spot sizes and rep rates, that samples with $\ll 1$ ppb U can be analyzed. Third, older samples—
238 when run on the *P3D*—reach their best possible uncertainty with U concentrations of 10–15 ppb; samples
239 as young as 80 Ma require little more than 30 ppb U, and samples as young as 15 Ma require up to 150
240 ppb U at moderate spot sizes. Though 2% final uncertainty requires greater concentrations of U for
241 younger samples (>2500 cps ^{238}U are needed for an 80 Ma sample, and $>12,000$ cps ^{238}U for a 15 Ma
242 sample), it should be noted that—at a given concentration, spot size and U/Pb_c —absolute uncertainty is
243 relatively independent of age; for example, a sample with a 65 μm spot and 10 ppb U yields an
244 uncertainty of just over 2 Ma, whether the sample is 15, 80, or 440 Ma. Finally, though not depicted
245 directly in Figure 6, precise ages can be obtained from data with rather low U/Pb_c values. For example,
246 100 spots with 2% uncertainty yields a final uncertainty of 5–15 Ma (2σ) for samples with U/Pb_c ratios as
247 low as 1–2. That said, data with such low U/Pb_c ratios should be viewed with caution, as systematic
248 uncertainties—such as those introduced by inconsistencies in RM isotopic measurements—can lead to
249 large errors when extrapolating data clustered near the upper intercept.



250 **4.3 More spots, deeper spots, or bigger spots?**

251 The theoretical models discussed above use a 10 sec integration time to compare the models to the
252 empirical data. As discussed above, precision can be improved by increasing the number of analytical
253 spots, but each spot can also be ablated for longer or at a higher rep rate (i.e., making deeper pits rather
254 than more pits). One might imagine that these methods might be equally effective, however, there are two
255 important points to consider. First, individual spot precision is limited to the long-term reproducibility of
256 down-hole measurements, and is generally no better than 2%; this precision is more difficult to assess in
257 calcite because most known reference materials exhibit moderate isotopic heterogeneity (e.g., Roberts et
258 al., 2017). Thus, if increasing the depth of the pit yields analytical uncertainties <2%, then the excess pit
259 depth is wasted and overall uncertainty fails to improve. Second, whereas increasing the number of spots
260 leads to a linear increase in the total number of counts (and thus an increase in precision by \sqrt{n}), an
261 increase in pit depth does not lead to a linear increase in counts because ablation yields decrease with pit
262 depth. Thus, if an increase in total counts could yield better precision, that increase should come from
263 more, shallower laser pits, rather than fewer, deeper pits.

264 It is also possible to increase precision by increasing the spot size. In fact, an argument could be made
265 that a SC-ICPMS that measures 250 μm spots is just as effective as a MC-ICPMS that measures 100 μm
266 spots. Though this argument has merit, the downside is twofold; 1) some regions of interest are simply
267 not large enough to permit a spot 2.5X as wide, and 2) U and/or Pb (i.e., U/Pb_c) may be heterogeneous at
268 scales smaller than the spot size, mixing calcite of different age or reducing the range of isotopic ratios
269 that are used to construct an isochron. Figure 7 demonstrates that even though larger spots can yield a
270 better per-spot precision, analyzing the same volume of material with smaller spots can yield better age
271 precision because it can take advantage of the heterogeneous U and Pb concentrations typical of calcite.



272 5 Conclusions

273 1) Unlike geochronometers with high U and little to no common Pb—such as zircon and monazite—U-Pb
274 dates of minerals with low U and significant common Pb can be limited by the count rates of the parent
275 U, rather than the daughter Pb.

276 2) Given a limit of detection of ~8000 cps for on a Faraday, and the sensitivity of the *Nu P3D*, samples
277 with as low as 20 ppb U can be analyzed with a 100 μm spot at 10 Hz, and as low as 5 ppb for a 200 μm
278 spot. Even so, the Faraday is less precise than the Daly at count rates of <30,000 cps, corresponding to U
279 concentrations of ca. 75 and 20 ppb, with the same respective spot sizes and rep rates.

280 3) When ^{238}U is analyzed on a Daly, the limit of detection drops by a factor of >1000, and the analytical
281 capability is thus limited by the LOD of Pb— ^{207}Pb in almost all cases—and the ratio required for
282 optimum precision. The typical LOD of ^{206}Pb and ^{207}Pb is ca. 50 cps; it is greater for higher sensitivity
283 instruments, and those with a higher background of common Pb. For a desired U/Pb_c ratio of ca. 5–10 for
284 old and young samples, respectively, the required count rate of ^{238}U would be 500–1000 cps or ca. 5–10
285 times smaller than can be analyzed on a Faraday detector. The analysis of ^{238}U on a Daly, therefore
286 increases the analytical capability to ca. 0.5–2 ppb U for a 100–200 μm spot, respectively.

287 4) Although the % uncertainty that can be achieved with limited concentrations of U is considerably
288 different among samples with different ages, the absolute uncertainty is approximately the same. For
289 example, samples with 1500 cps ^{238}U yield a maximum possible uncertainty of ca. 2 Ma, nearly
290 independent of age (older samples yield slightly higher absolute uncertainties). However, because most
291 LA-ICPMS facilities can achieve up to 2% precision on final age calculations, younger samples can yield
292 better absolute uncertainties; these can only be achieved at high U concentrations, which limits the
293 advantage of the *Nu P3D* for young samples.

294 5) Given enough material and analytical time, a SC-ICPMS, should, in theory, be capable of measuring
295 samples with concentrations of approximately 2–10 times (i.e., 1–20 ppb U) that of the *Nu P3D*.



296 However, because of their lower cycle times and inability to make concurrent measurements, SC-ICPMS
297 instruments likely require considerably higher concentrations of U to obtain comparable date precision.

298 Figure Captions

299 Figure 1. Relation between cps ^{238}U and uncertainty of ^{238}U (A), and $^{206}\text{Pb}/^{238}\text{U}$ (B). The 3 experiments
300 show the same trend in uncertainty vs. cps at count rates above ~ 30 kcps ^{238}U , but below that, uncertainty
301 of measurements in Experiment F (238 on the Faraday) increase significantly compared to Experiments D
302 and Q. Although Experiments D and Q (red and blue symbols) show the similar trends, the sensitivity
303 gain using the P3D leads to significant improvements in spot uncertainty (large symbols represent
304 expected uncertainties for a 100 μm spot at 10 ppb U).

305 Figure 2. Tera–Wasserburg concordia diagrams of the 3 unknown samples in each of the 3 experiments.
306 See text for discussion.

307 Figure 3. Uncertainty ellipses for each Tera–Wasserburg plot depict the counting uncertainty for 10 s at a
308 given ^{238}U count rate for different U/Pbc ratios of 1, 2, 5, 10, 20, 50, 100, 200. For each U/Pbc, the larger
309 ellipse is the limit of detection for the all-Daly configuration, or any SC-ICPMS (limited by ^{207}Pb counts).
310 The smaller, red ellipse indicates the uncertainty at 30,000 cps ^{238}U , the point at which the measurement
311 of ^{238}U on the Daly is no longer advantageous.

312 Figure 4. Left-hand plots show the difference in distribution of $^{238}\text{U}/^{206}\text{Pb}$ ratios in reference materials and
313 unknowns; ratios are normalized to the $^{238}\text{U}/^{206}\text{Pb}$ ratio of the age of the sample. Reference materials Duff
314 Brown and WC-1 have the smallest variation in $^{238}\text{U}/^{206}\text{Pb}$ ratios, which correlates well with the
315 distribution of their U and Pb contents (left-hand plots). Reference material ASH15 and unknown sample
316 C283C still have a wider log-normal distribution, reflective of their larger distribution of U and Pb
317 contents relative to Duff Brown and WC-1. Unknown sample C273C has a more uniform distribution of
318 $^{238}\text{U}/^{206}\text{Pb}$ ratios, reflecting its largest distribution of U contents.



319 Figure 5. A-C shows an example of the differing randomly generated distributions of 100 analyses with
320 the same maximum U/Pb_c . 5A shows a normal distribution for the entire range of U/Pb_c ; 5B is a normal
321 distribution over the upper 50% of the same range. The uniform distribution, shown in 5C, yields the
322 lowest uncertainties because there are more analyses at both the upper and lower intercepts. D shows how
323 the percent uncertainty decreases with number of analyses, depending on the type of $^{238}U/^{206}Pb$
324 distribution depicted in A–C; data in D assumed the best case scenario of 2% uncertainty per data point
325 and a U/Pb_c ratio of 10 for samples of 440 Ma, 80 Ma, and 15 Ma. Best uncertainties are achieved with
326 uniform distributions and maximum spread. Although percent uncertainties are always better for older
327 samples, younger samples yield better absolute uncertainties for well distributed data.

328 Figure 6. 6A shows the count rate expected with the Nu P3D given for a given spot size at a laser energy
329 of ~ 1 J/cm² and 10 Hz. Spots indicate analyses of unknowns in Experiment F (^{238}U on the Faraday; color
330 represents the maximum U/Pb_c ratio—taken from Table 2—and the size represents the uncertainty). Dark
331 grey area is below the LOD for ^{238}U on a Faraday; the light grey area represents ^{238}U count rates favorably
332 measured on the Daly detector. Figures B, D, and F show the maximum possible U/Pb_c ratio that can be
333 detected, given a minimum count rate of 30 cps for ^{207}Pb at different sample ages. C, E, and G show the
334 best possible uncertainty at the given count rates and spot sizes for 100 analyses, all with the same U
335 concentration but a uniform distribution of $^{238}U/^{206}Pb$ ratios.

336 Figure 7. Tera–Wasserburg diagram representing the analysis of a heterogeneous medium using different
337 spot sizes. Though the bigger spot sizes yield smaller individual uncertainties, the smaller spots take
338 advantage of the spread in U/Pb_c ratios and thus yield a better overall uncertainty on the lower intercept
339 age.

340

341 Burisch, M., Gerdes, A., Walter, B. F., Neumann, U., Fettel, M., and Markl, G.: Methane and the origin
342 of five-element veins: Mineralogy, age, fluid inclusion chemistry and ore forming processes in the
343 Odenwald, SW Germany, *Ore Geology Reviews*, 81, 42-61, 10.1016/j.oregeorev.2016.10.033, 2017.



- 344 Chew, D. M., Petrus, J. A., and Kamber, B. S.: U-Pb LA-ICPMS dating using accessory mineral
345 standards with variable common Pb, *Chemical Geology*, 363, 185-199, 10.1016/j.chemgeo.2013.11.006,
346 2014.
- 347 Goodfellow, B. W., Viola, G., Bingen, B., Nuriel, P., and Kylander-Clark, A. R.: Palaeocene faulting in
348 SE Sweden from U-Pb dating of slickenfibres calcite, *Terra Nova*, 29, 321-328, 2017.
- 349 Hill, C. A., Polyak, V. J., Asmerom, Y., and P. Provencio, P. C. T. C.: Constraints on a Late Cretaceous
350 uplift, denudation, and incision of the Grand Canyon region, southwestern Colorado Plateau, USA, from
351 U-Pb dating of lacustrine limestone, *Tectonics*, 35, 896-906, 10.1002/2016tc004166, 2016.
- 352 Hoff, J. A., Jameson, J., and Hanson, G. N.: Application of Pb Isotopes to the Absolute Timing of
353 Regional Exposure Events in Carbonate Rocks - an Example from U-Rich Dolostones from the Wahoo
354 Formation (Pennsylvanian), Prudhoe Bay, Alaska, *Journal of Sedimentary Research Section a-
355 Sedimentary Petrology and Processes*, 65, 225-233, 1995.
- 356 Horstwood, M. S. A., Košler, J., Gehrels, G., Jackson, S. E., McLean, N. M., Paton, C., Pearson, N. J.,
357 Sircombe, K., Sylvester, P., Vermeesch, P., Bowring, J. F., Condon, D. J., and Schoene, B.: Community-
358 Derived Standards for LA-ICP-MS U-(Th)-Pb Geochronology – Uncertainty Propagation, Age
359 Interpretation and Data Reporting, *Geostandards and Geoanalytical Research*, 10.1111/j.1751-
360 908X.2016.00379.x, 2016.
- 361 Manganot, X., Gasparrini, M., Gerdes, A., Bonifacie, M., and Rouchon, V.: An emerging
362 thermochronometer for carbonate-bearing rocks: Delta(47)/(U-Pb), *Geology*, 46, 1067-1070,
363 10.1130/G45196.1, 2018.
- 364 Nuriel, P., Weinberger, R., Kylander-Clark, A. R., Hacker, B., and Craddock, J.: The onset of the Dead
365 Sea transform based on calcite age-strain analyses, *Geology*, 45, 587-590, 2017.
- 366 Nuriel, P., Wotzlaw, J.-F., Stremtan, C., Vaks, A., and Kylander-Clark, A. R.: The use of ASH15
367 flowstone as matrix-matched standard for laser-ablation geochronology of calcite, *Geochronology*, 2, in
368 review.
- 369 Paton, C., Hellstrom, J., Paul, B., Woodhead, J., and Hergt, J.: Iolite: Freeware for the visualisation and
370 processing of mass spectrometric data, *Journal of Analytical Atomic Spectrometry*, 26, 2508-2518,
371 10.1039/c1ja10172b, 2011.
- 372 Rasbury, E. T., Hanson, G. N., Meyers, W. J., and Saller, A. H.: Dating of the time of sedimentation
373 using U-Pb ages for paleosol calcite, *Geochimica Et Cosmochimica Acta*, 61, 1525-1529, Doi
374 10.1016/S0016-7037(97)00043-4, 1997.
- 375 Rasbury, E. T., Hanson, G. N., Meyers, W. J., Holt, W. E., Goldstein, R. H., and Saller, A. H.: U-Pb dates
376 of paleosols: Constraints on late Paleozoic cycle durations and boundary ages, *Geology*, 26, 403-406, Doi
377 10.1130/0091-7613(1998)026<0403:Updopc>2.3.Co;2, 1998.
- 378 Richards, D. A., Bottrell, S. H., Cliff, R. A., Strohle, K., and Rowe, P. J.: U-Pb dating of a speleothem of
379 Quaternary age, *Geochimica Et Cosmochimica Acta*, 62, 3683-3688, Doi 10.1016/S0016-7037(98)00256-
380 7, 1998.
- 381 Roberts, N. M. W., and Walker, R. J.: U-Pb geochronology of calcite-mineralized faults: Absolute timing
382 of rift-related fault events on the northeast Atlantic margin, *Geology*, 44, 531-534, 10.1130/G37868.1,
383 2016.
- 384 Roberts, N. M. W., Rasbury, E. T., Parrish, R. R., Smith, C. J., Horstwood, M. S. A., and Condon, D. J.:
385 A calcite reference material for LA-ICP-MS U-Pb geochronology, *Geochemistry Geophysics
386 Geosystems*, 18, 2807-2814, 10.1002/2016GC006784, 2017.
- 387 Spencer, K. J., Hacker, B. R., Kylander-Clark, A. R. C., Andersen, T. B., Cottle, J. M., Stearns, M. A.,
388 Poletti, J. E., and Seward, G. G. E.: Campaign-style titanite U-Pb dating by laser-ablation ICP:
389 Implications for crustal flow, phase transformations and titanite closure, *Chemical Geology*, 341, 84-101,
390 10.1016/j.chemgeo.2012.11.012, 2013.
- 391 Wang, Z. S., Rasbury, E. T., Hanson, G. N., and Meyers, W. J.: Using the U-Pb system of calcretes to
392 date the time of sedimentation of elastic sedimentary rocks, *Geochimica Et Cosmochimica Acta*, 62,
393 2823-2835, Doi 10.1016/S0016-7037(98)00201-4, 1998.



394 Winter, B. L., and Johnson, C. M.: U-Pb Dating of a Carbonate Subaerial Exposure Event, Earth and
395 Planetary Science Letters, 131, 177-187, Doi 10.1016/0012-821x(95)00026-9, 1995.
396
397



Table 1.

Instrumental parameters of laser-ablation split-stream ICP-MS

	MC-ICP-MS	Q-ICP-MS
Instrument model	Nu Plasma 3D	Agilent 7700x
RF forward power	1300 W	1300 W
RF reflected power	<10 W	<10 W
Coolant gas	13 L/min	13 L/min
Auxiliary gas	0.8 L/min	0.8 L/min
Make up gas	~1 L/min	~1 L/min
Monitored masses (dwell times listed for <i>Agilent</i>)	²³⁸ U, ²³² Th, ²⁰⁸ Pb, ²⁰⁷ Pb, ²⁰⁶ Pb, ²⁰⁴ Pb/ ²⁰⁴ Hg, ²⁰² Hg	²³⁸ U(0.06), ²⁰⁷ Pb (0.13), ²⁰⁶ Pb (0.1), ²⁰⁴ Pb/ ²⁰⁴ Hg (0.1)
²³⁸ U sensitivity, dry solution	0.5% (23 Mcps/ppb)	0.1% (4 Mcps/ppb)
<u>Laser-Ablation System</u>		
Instrument model	Photon Machines Analyte 193	
Laser	ATLEX-SI 193nm ArF excimer	
Fluence	~1 J/cm ²	
Repetition rate	10 Hz	
Excavation rate	~0.07 μm/pulse	
Spot size	65–110 μm	
Delay between analyses	20 s	
Ablation duration	15 s	
Carrier gas (He) flow (cell; cup)	0.12; 0.06 L/min	



Table 2. Results from 3 experiments

sample #	C258	C273C	C304A	C283A	C283C	C254A
Experiment F (P3D - 238 on Faraday; 65 μm, ~ 2.7 mV/ppm U)						
total spots	110	100	100	100	100	100
$^{238}\text{U}/^{206}\text{Pb}$ $2\sigma < 50\%$	54%	76%	63%	29%	38%	63%
spots for isochron	35%	76%	47%	21%	25%	n/a
average U ppb	40	195	286	28	25	456
median U ppb	30	73	96	25	27	55
average cps 238	7100	33800	46800	4600	4100	73100
median cps 238	5300	12700	15700	4100	4400	8800
avg. $^{238}\text{U}/^{206}\text{Pb}$ 2σ	28%	17%	17%	32%	35%	24%
maximum U/Pb _c	49	145	54	27	17	n/a
Age (Ma)	437 \pm 18	80.9 \pm 1.5	111.1 \pm 2.1	453 \pm 40	492 \pm 81	n/a
final 2σ	4.1%	1.9%	1.9%	8.8%	16.5%	n/a
Experiment D (P3D - 238 on Daly; 65 μm, ~ 2.1–2.7 mV/ppm U)						
total spots	100	100	100	100	100	100
$^{238}\text{U}/^{206}\text{Pb}$ $2\sigma < 50\%$	96%	98%	97%	97%	93%	90%
spots for isochron	75%	90%	84%	64%	68%	n/a
average U ppb	24	144	196	11	18	232
median U ppb	13	59	40	8	18	33
average cps 238	3800	24500	27900	1600	2400	29300
median cps 238	2100	10000	5700	1200	2400	4200
avg. $^{238}\text{U}/^{206}\text{Pb}$ (2σ)	16%	10%	12%	17%	16%	19%
maximum U/Pb _c	30	205	79	26	12	n/a
Age (Ma)	445 \pm 11	83.5 \pm 1.6	119.3 \pm 2.3	430 \pm 11	430 \pm 14	n/a
final 2σ	2.5%	1.9%	1.9%	2.6%	3.3%	n/a
Experiment Q (Agilent 7700 Q-ICPMS; 110 μm, ~ 1.8 mV/ppm U)						
total spots	110	100	100			
$^{238}\text{U}/^{206}\text{Pb}$ $2\sigma < 50\%$	96%	87%	94%			
spots for isochron	75%	87%	94%			
average U ppb	28	126	371			
median U ppb	14	68	80			
average cps 238	3100	14400	39400			
median cps 238	1600	7800	8500			
avg. $^{238}\text{U}/^{206}\text{Pb}$ (2σ)	20%	14%	13%			
maximum U/Pb _c	26	325	93			
Age (Ma)	460 \pm 18	85.4 \pm 2.0	118.1 \pm 4.0			
final 2σ	3.9%	2.3%	3.4%			

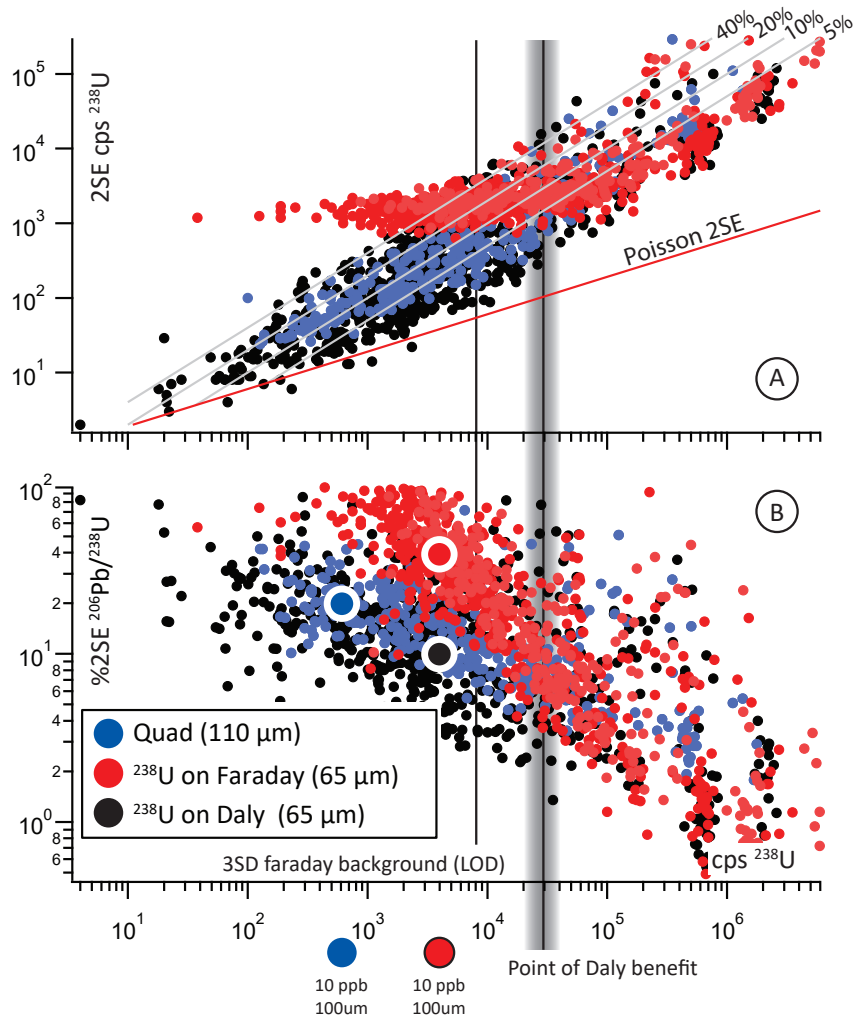


Figure 1. Relation between cps ^{238}U and uncertainty of ^{238}U (A), and $^{206}\text{Pb}/^{238}\text{U}$ (B). The 3 experiments show the same trend in uncertainty vs. cps at count rates above ~ 30 kcps ^{238}U , but below that, uncertainty of measurements in Experiment F (^{238}U on the Faraday) increase significantly compared to Experiments D and Q. Although Experiments D and Q (red and blue symbols) show the similar trends, the sensitivity gain using the P3D leads to significant improvements in spot uncertainty (large symbols represent expected uncertainties for a 100 μm spot at 10 ppb U).

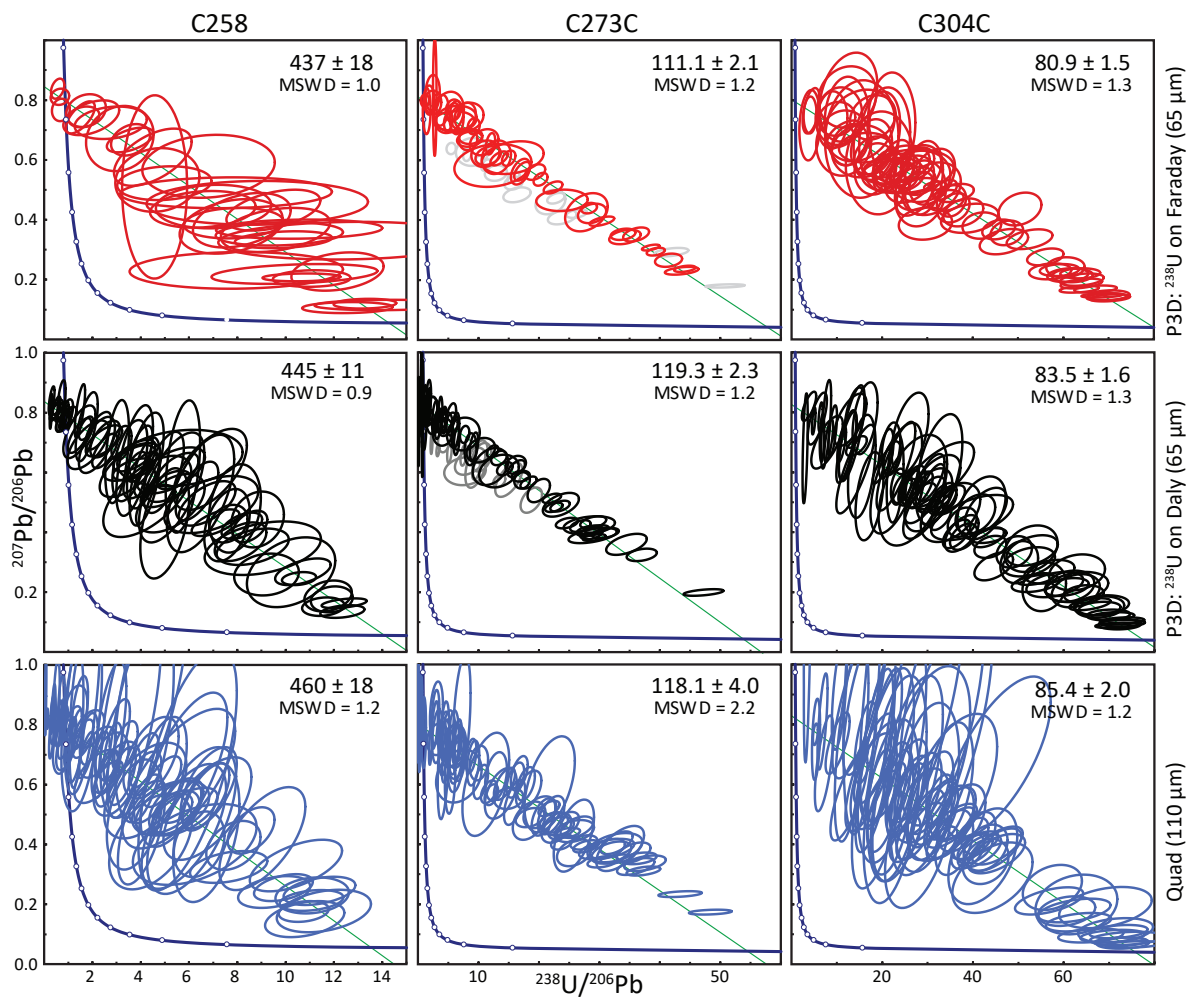


Figure 2. Tera–Wasserburg concordia diagrams of the 3 unknown samples in each of the 3 experiments. See text for discussion.

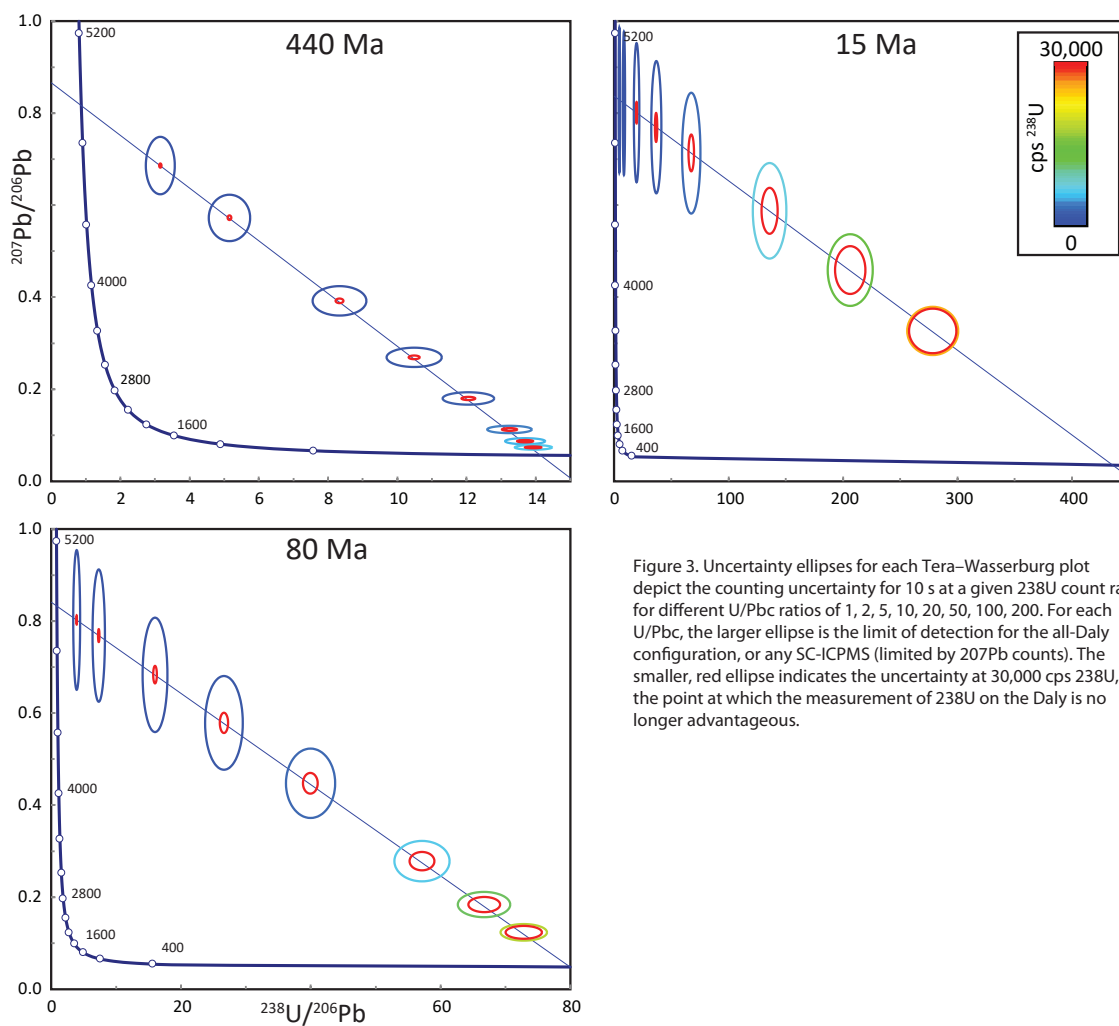


Figure 3. Uncertainty ellipses for each Tera-Wasserburg plot depict the counting uncertainty for 10 s at a given ^{238}U count rate for different U/Pbc ratios of 1, 2, 5, 10, 20, 50, 100, 200. For each U/Pbc, the larger ellipse is the limit of detection for the all-Daly configuration, or any SC-ICPMS (limited by ^{207}Pb counts). The smaller, red ellipse indicates the uncertainty at 30,000 cps ^{238}U , the point at which the measurement of ^{238}U on the Daly is no longer advantageous.

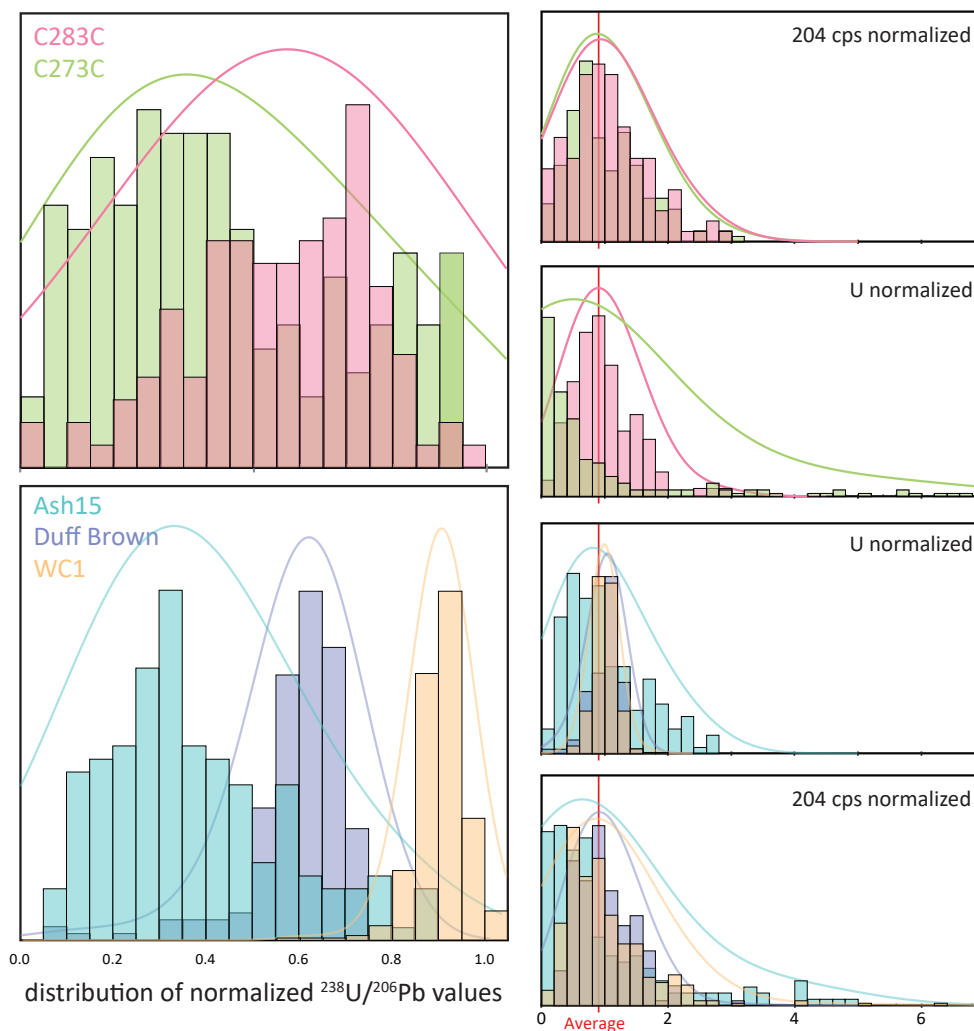


Figure 4. Left-hand plots show the difference in distribution of $^{238}\text{U}/^{206}\text{Pb}$ ratios in reference materials and unknowns; ratios are normalized to the $^{238}\text{U}/^{206}\text{Pb}$ ratio of the age of the sample. Reference materials Duff Brown and WC-1 have the smallest variation in $^{238}\text{U}/^{206}\text{Pb}$ ratios, which correlates well with the distribution of their U and Pb contents (left-hand plots). Reference material ASH15 and unknown sample C283C still have a wider log-normal distribution, reflective of their larger distribution of U and Pb contents relative to Duff Brown and WC-1. Unknown sample C273C has a more uniform distribution of $^{238}\text{U}/^{206}\text{Pb}$ ratios, reflecting its largest distribution of U contents.

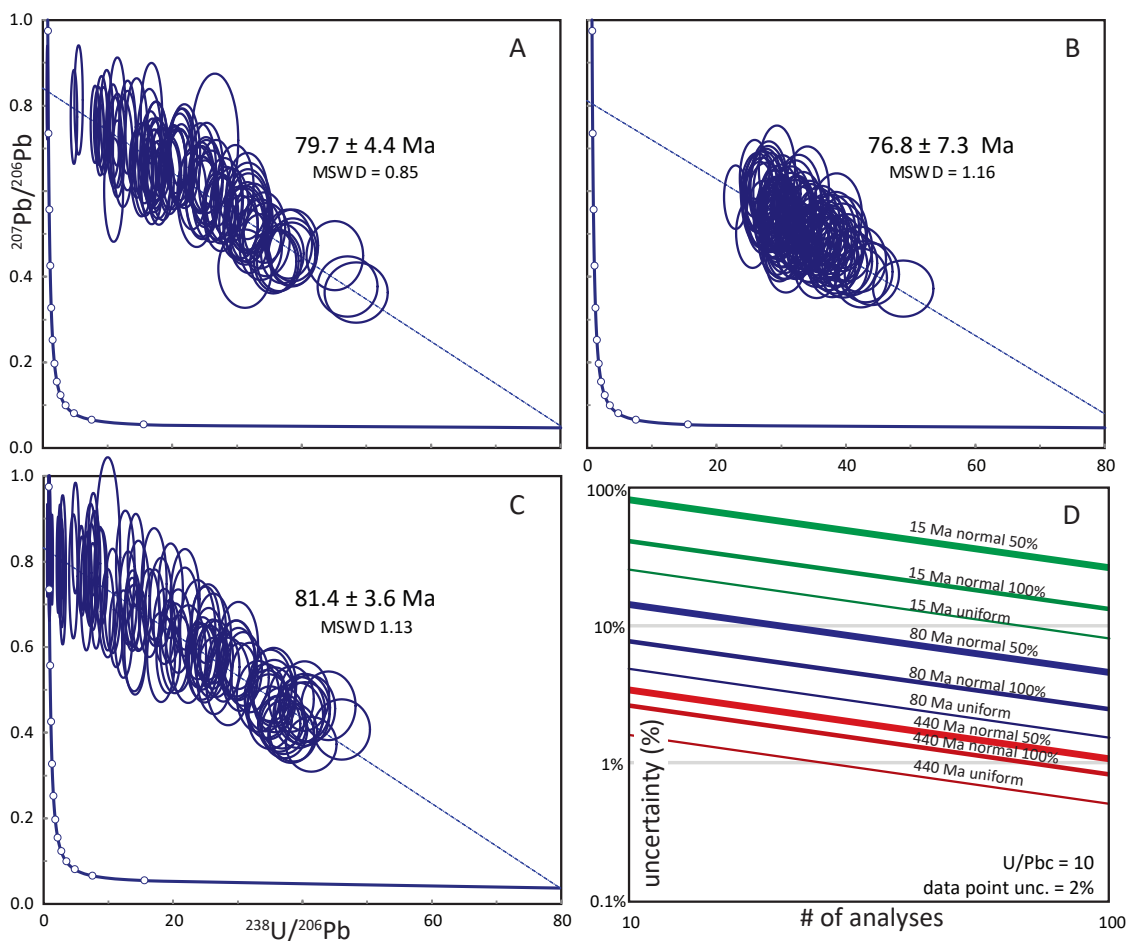


Figure 5. A-C shows an example of the differing randomly generated distributions of 100 analyses with the same maximum U/Pbc. 5A shows a normal distribution for the entire range of U/Pbc; 5B is a normal distribution over the upper 50% of the same range. The uniform distribution, shown in 5C, yields the lowest uncertainties because there are more analyses at both the upper and lower intercepts. D shows how the percent uncertainty decreases with number of analyses, depending on the type of $^{238}\text{U}/^{206}\text{Pb}$ distribution depicted in A–C; data in D assumed the best case scenario of 2% uncertainty per data point and a U/Pbc ratio of 10 for samples of 440 Ma, 80 Ma, and 15 Ma. Best uncertainties are achieved with uniform distributions and maximum spread. Although percent uncertainties are always better for older samples, younger samples yield better absolute uncertainties for well distributed data.

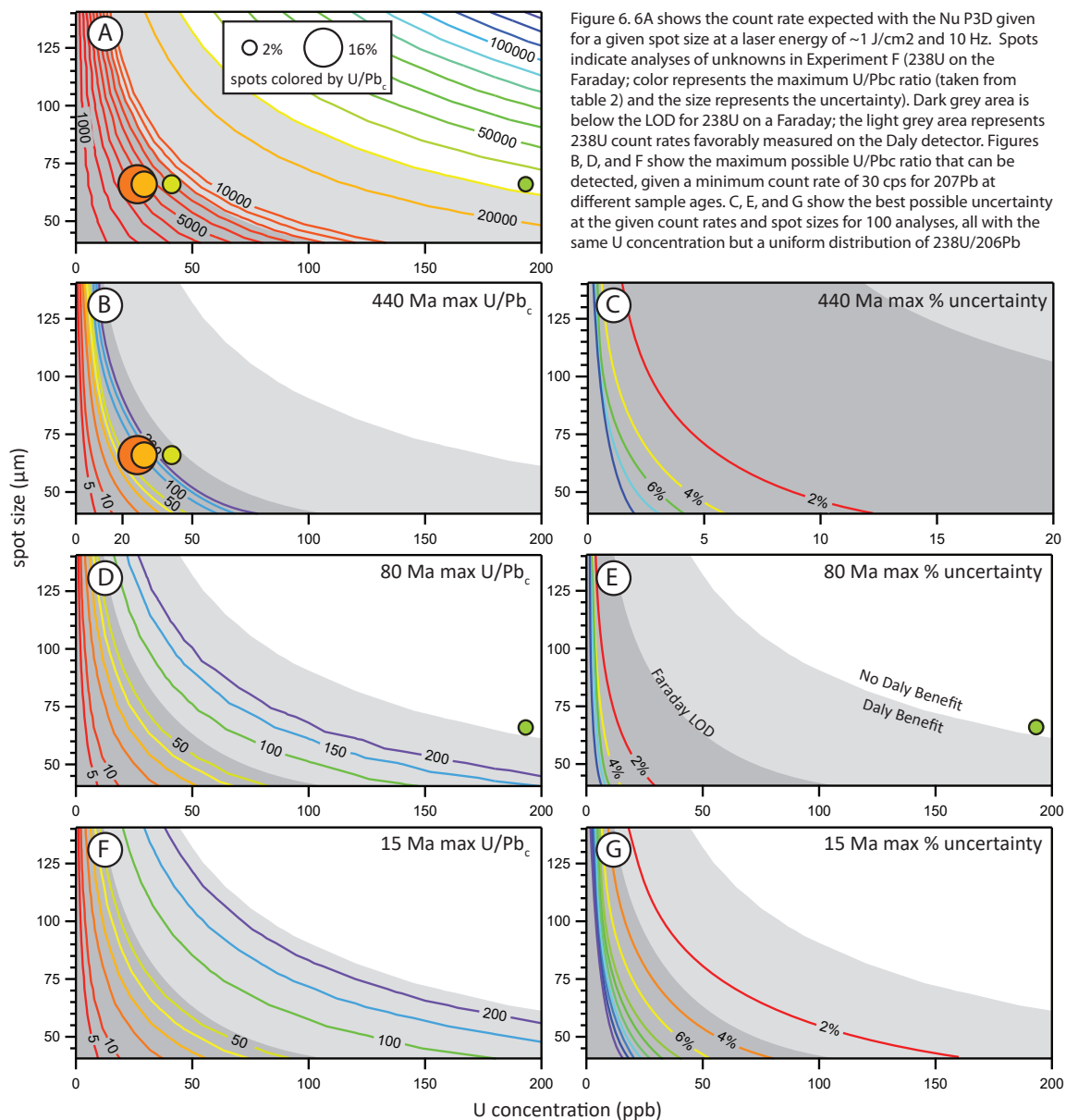


Figure 6. 6A shows the count rate expected with the Nu P3D given for a given spot size at a laser energy of $\sim 1 \text{ J/cm}^2$ and 10 Hz. Spots indicate analyses of unknowns in Experiment F (^{238}U on the Faraday; color represents the maximum U/Pb_c ratio (taken from table 2) and the size represents the uncertainty). Dark grey area is below the LOD for ^{238}U on a Faraday; the light grey area represents ^{238}U count rates favorably measured on the Daly detector. Figures B, D, and F show the maximum possible U/Pb_c ratio that can be detected, given a minimum count rate of 30 cps for ^{207}Pb at different sample ages. C, E, and G show the best possible uncertainty at the given count rates and spot sizes for 100 analyses, all with the same U concentration but a uniform distribution of $^{238}\text{U}/^{206}\text{Pb}$

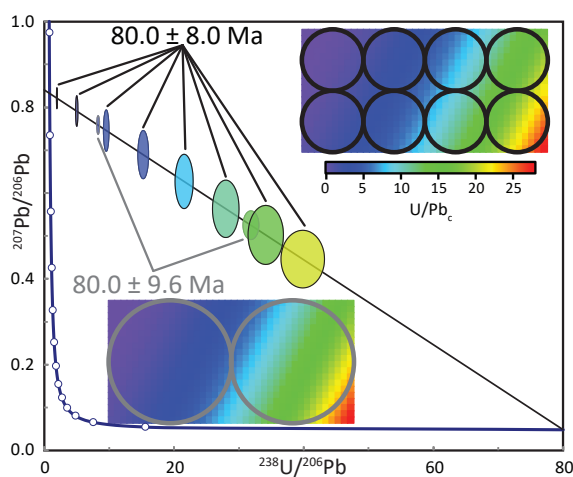


Figure 7. Tera–Wasserburg diagram representing the analysis of a heterogeneous medium using different spot sizes. Though the bigger spot sizes yield smaller individual uncertainties, the smaller spots take advantage of the spread in U/Pbc ratios and thus yield a better overall uncertainty on the lower intercept age.